IRS-Assisted Short Packet Wireless Energy Transfer and Communications

Bingxin Zhang, *Student Member, IEEE*, Kezhi Wang, *Senior Member, IEEE*, Kun Yang, *Senior Member, IEEE*, and Guopeng Zhang

***Abstract*—In this paper, we analyse and optimize an intelligent reflecting surface (IRS)-assisted ultra-reliable and low-latency communications (uRLLC) system supported by wireless energy transfer (WET) technology, in which short packets are used in both the WET and wireless information transfer (WIT) phases. We first present the statistical features of the signal-to-noise-ratio (SNR) of the system. Then, we derive an approximate closed-form expression of the average packet error probability (APEP). Additionally, we optimize the channel uses in the WET and WIT phases to maximize the effective throughput (ET) of the system. Finally, the effectiveness of the proposed solution is verified by Monte-Carlo simulation.**

***Index Terms*—Average Packet Error Probability, Effective Throughput, Short-Packet Communications, Wireless Energy Transfer, uRLLC**

I. Introduction

Internet of Things (IoT) has become a key enabler of 5G networks to support large-scale connection among devices or machines [1]. However, most of the IoT applications require ultra-reliable and low-latency communications (uRLLC). For example, the maximum latency of factory automation varies from 250 μs to 10 ms, and the maximum error probability is 10^{-9}. Therefore, the IoT network may require short packets with finite blocklength coding (FBC) to reduce physical layer transmission delay. On the other hand, IoT devices are usually powered by batteries with limited energy supply. To this end, wireless energy transfer (WET) is applied to provide energy for low-power IoT devices through radio frequency [2]. Also, the IoT network supported by WET technology will likely make exclusive use of short packets due to the inherently small data payload and low latency requirements [3]. In [4], the authors derived an approximate expression to describe the performance of error probability and delay in the ultra-reliable communication scenarios. Nevertheless, in the millimeter wave (mmWave) or higher frequency band, the signal will be more susceptible to blockage. Therefore, we need to overcome the uncontrollable effects of wireless channel to ensure reliable information or energy transfer.

Recently, intelligent reflecting surface (IRS) has attracted much attention by controlling the wireless propagation environment via adjusting phase and/or amplitude response of the meta-surface, which can significantly improve the spectrum and energy efficiency of the system [5]. In [6], the authors investigated the coverage of RIS-aided large-scale mmWave cellular network, in which base stations, RISs and users are randomly distributed in a 2-dimensional space. The authors in [7] studied the weighted sum rate maximization problems of all users in multicell by jointly optimizing the transmit beamforming of base stations and the phase offset of IRS. The authors in [8] considered a prefabricated RIS-empowered wall architecture to ensure reliable outdoor-to-indoor communication in mmWave cellular networks. The superiority of IRS in uRLLC or WET systems have been studied. In [9], the authors investigated the performance of a reconfigurable intelligent surface assisted uRLLC system by analysing the average achievable rate and error probability. The authors in [10] considered an IRS-aided multiple-input multiple-output wireless powered communication networks in which the IRS adjust their phase shifts to maximize the system throughput. However, none of the above works considered the IRS-assisted uRLLC system supported by WET technology. Nevertheless, this is important for the future low-power IoT systems which required low-latency and high-relatability communications.

Against the above background, this paper considers an IRS-assisted uRLLC system supported by WET technology, in which short packets are used in the wireless information transfer (WIT) and WET phases. The system can be applied to IoT scenarios with a large number of low-power devices such as in automated factories, smart homes, intelligent transportation and e-health scenarios. The key contributions of our work are summarized as follows:

- We derive the closed-form expression of probability density function (PDF) and cumulative distribution function (CDF) of the instantaneous signal-to-noise ratio (SNR) at the HAP.
- Next, we analyse the performance of the average packet error probability (APEP) and derive an approximate expressions via linear function approximation.

Manuscript received September 22, 2021; accepted November 5, 2021. This work was supported by the National Natural Science Foundation of China under Grant 61620106011, Grant U1705263, Grant 61871076 and Grant 61971421. The associate editor coordinating the review of this article and approving it for publication was J. Choi. *(Corresponding author: Guopeng Zhang.)*

Bingxin Zhang is with the School of Information and Communication Engineering, University of Electronic Science and Technology of China (UESTC), Chengdu 611731, China, and also with the Yangtze Delta Region Institute (Huzhou) of UESTC, Zhejiang, China (e-mail: bxzhang@std.uestc.edu.cn).

Kezhi Wang is with the Department of Computer and Information Sciences, Northumbria University, Newcastle upon Tyne NE1 8ST, U.K. (e-mail: kezhi.wang@northumbria.ac.uk).

Kun Yang is with the Yangtze Delta Region Institute (Quzhou) & School of Information and Communication Engineering, University of Electronic Science and Technology of China, Quzhou 324000, China, and Changchun Institute of Engineering, Jilin, China (e-mail: kunyang@uestc.edu.cn).

Guopeng Zhang is with the School of Computer Science and Technology, China University of Mining and Technology, Xuzhou 221116, China (e-mail: gpzhang@cumt.edu.cn).

• Then, based on the derived APEP, we formulate the effective throughput (ET) maximization problem and propose a genetic algorithm (GA) based solution to find the best channel uses in the WET and WIT phases.

II. System Model and Statistical Features

As depicted in Fig. 1, we consider an IRS-assisted uRLLC scenario supported by WET technology, which consists a HAP, a device node, and an IRS with N reflecting elements. The "harvest-then-transmit" protocol is implemented, where in the WET phase, the HAP charges the device during m channel uses. Then, in the WIT phase, the device uses all the energy obtained to transmit L information bits over v channel uses. The duration of a channel use is represented by T_c.

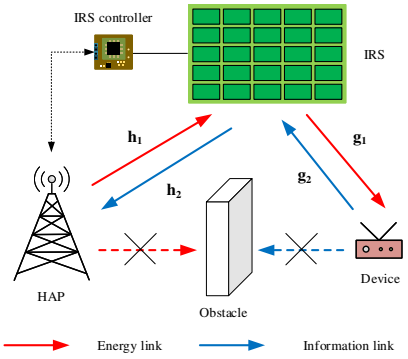

Fig. 1. The IRS-assisted uRLLC system supported by WET technology, where short packets are used in the WET and WIT phases.

It is assumed that the links between the HAP and device can only be established through the IRS, while the direct links is weak or blocked due to severe blockage. The HAP and device are equipped with a single antenna and operate in the half-duplex mode. We assume that all the channels experience independent Rayleigh fading [1]. The complex coefficient vectors from the HAP to IRS, from the IRS to HAP, from the IRS to device and from the device to IRS are represented as $\mathbf{h}_1 = [h_{1,1}, ..., h_{1,N}]^{\mathrm{H}}$, $\mathbf{h}_2 = [h_{2,1}, ..., h_{2,N}]^{\mathrm{H}}$, $\mathbf{g}_1 = [g_{1,1}, ..., g_{1,N}]^{\mathrm{H}}$ and $\mathbf{g}_2 = [g_{2,1}, ..., g_{2,N}]^{\mathrm{H}}$, respectively. We assume that the channel fading is independent and identically distributed (i.i.d.) and keep unchanged during the WET or WIT phases. Then, we consider $h_{1,n}, h_{2,n} \sim \mathcal{CN}(0, \alpha)$ and $g_{1,n}, g_{2,n} \sim \mathcal{CN}(0, \beta)$, where α and β are fading coefficients.

In the WET phase, the diagonal reflection-coefficient matrix at the IRS is $\mathbf{\Phi}_{\mathrm{E}} = \mathrm{diag}(e^{j\phi_1^{\mathrm{E}}}, ..., e^{j\phi_N^{\mathrm{E}}})$, where $\phi_n^{\mathrm{E}} \in [0, 2\pi)$ is the phase shift of the n-th reflecting element. It is assumed that the signal power reflected by the IRS more than once can be ignored. Then, the amount of energy harvested by the device during the WET phase is given as follows

$$E_{\mathrm{E}} = \eta m T_c P_t ||\mathbf{h}_1^{\mathrm{H}} \mathbf{\Phi}_{\mathrm{E}} \mathbf{g}_1||^2, \tag{1}$$

where $0 < \eta < 1$ is the energy harvesting efficiency of the device, P_t is the transmit power at HAP, and mT_c is the time that the HAP charges the device by sending short packets.

[1]In this paper, we consider that the IRS is large enough. Therefore, the channel correlation is ignored for analytical tractability [8], [11].

Then, in the WIT phase, the device uses all the energy obtained to transmit L information bits over v channel uses. The received signal at the HAP can be written as

$$\begin{aligned} y_{\mathrm{I}} &= \sqrt{\frac{E_{\mathrm{E}}}{vT_c}} \mathbf{g}_2^{\mathrm{H}} \mathbf{\Phi}_{\mathrm{I}} \mathbf{h}_2 x_{\mathrm{I}} + w_{\mathrm{I}} \\ &= \sqrt{\frac{\eta m T_c P_t}{vT_c}} \cdot \mathbf{h}_1^{\mathrm{H}} \mathbf{\Phi}_{\mathrm{E}} \mathbf{g}_1 \cdot \mathbf{g}_2^{\mathrm{H}} \mathbf{\Phi}_{\mathrm{I}} \mathbf{h}_2 \cdot \ x_{\mathrm{I}} + w_{\mathrm{I}}, \end{aligned} \tag{2}$$

where x_{I} is the information symbol with $\mathbb{E}[||x_{\mathrm{I}}||^2] = 1$, vT_c is the data transmission time by sending short packets, w_{I} is the additive white Gaussian noise (AWGN) at the HAP with zero mean and variance of σ_{I}^2, and $\mathbf{\Phi}_{\mathrm{I}} = \mathrm{diag}(e^{j\phi_1^{\mathrm{I}}}, ..., e^{j\phi_N^{\mathrm{I}}})$, $\phi_n^{\mathrm{I}} \in [0, 2\pi)$.

Then, the instantaneous SNR at the HAP is given by

$$\begin{aligned} \gamma &= \frac{\eta m P_t}{v\sigma_{\mathrm{I}}^2} ||\mathbf{h}_1^{\mathrm{H}} \mathbf{\Phi}_{\mathrm{E}} \mathbf{g}_1||^2 ||\mathbf{g}_2^{\mathrm{H}} \mathbf{\Phi}_{\mathrm{I}} \mathbf{h}_2||^2 \\ &= \delta \cdot \left| \sum_{n=1}^{N} h_{1,n} g_{1,n} e^{j\phi_n^{\mathrm{E}}} \right|^2 \cdot \left| \sum_{n=1}^{N} g_{2,n} h_{2,n} e^{j\phi_n^{\mathrm{I}}} \right|^2, \end{aligned} \tag{3}$$

where $\delta = \frac{\eta m P_t}{v\sigma_{\mathrm{I}}^2}$.

Furthermore, we assume that the channel state information (CSI) is known at the HAP. Channel estimation methods for communication with IRS can be found in [13]. Therefore, to maximize the received SNR, the IRS should carefully adjust the phase shift coefficients to satisfy $\phi_n^{\mathrm{E}} = -\arg(h_{1,n}) - \arg(g_{1,n})$, $\phi_n^{\mathrm{I}} = -\arg(h_{2,n}) - \arg(g_{2,n})$, $\forall n \in \{1, ..., N\}$. As a result, γ in (3) can be rewritten as

$$\gamma = \delta \cdot \left(\sum_{n=1}^{N} |h_{1,n}| \ |g_{1,n}| \right)^2 \cdot \left(\sum_{n=1}^{N} |g_{2,n}| \ |h_{2,n}| \right)^2, \tag{4}$$

III. Average Packet Error Probability

In the FBC region, the APEP of quasi-static fading channel can be approximated as [14]

$$\bar{\varepsilon} = \mathbb{E}[Q(g(\gamma))] = \int_0^{\infty} Q(g(\gamma)) f_{\gamma}(\gamma) \, d\gamma, \tag{5}$$

where $g(\gamma) = \ln 2 \sqrt{\frac{v}{V(\gamma)}} (\log_2(1+\gamma) - R_s)$, $R_s = \frac{L}{v}$ is the data rate, $V(\gamma) = 1 - \frac{1}{(1+\gamma)^2}$ is the channel dispersion, $Q(x) = \frac{1}{\sqrt{2\pi}} \int_x^{\infty} e^{-\frac{t^2}{2}} \, \mathrm{d}t$ is the Gaussian Q-function, and $f_{\gamma}(\gamma)$ is the PDF of SNR.

In order to get the APEP $\bar{\varepsilon}$ in (5), we need to identify the PDF of the SNR γ in (4). Let $\varrho_{1,n} = |h_{1,n}||g_{1,n}|$, $\varrho = \sum_{n=1}^{N} \varrho_{1,n}$, and we first derive the distribution of $\varrho_{1,n}$. However, it is difficult to derive the exact PDF of $\varrho_{1,n}$. To tackle this difficulty, we employ the moment matching technique to approximate $\varrho_{1,n}$ by Gamma distribution. The distribution of $\varrho_{1,n}$ can be approximated as [15]

$$f_{\varrho_{1,n}}(x) = \frac{1}{\Gamma(k) \theta^k} x^{k-1} \exp\left(-\frac{x}{\theta}\right), \tag{6}$$

where $k = \frac{\pi^2}{16 - \pi^2}$ is the shape parameter, $\theta = \frac{16 - \pi^2}{4\pi} \sqrt{\alpha\beta}$ is the scale parameter, and $\Gamma(\cdot)$ represents the Gamma function.

Since ϱ is the sum of N i.i.d. Gamma random variables with the parameters k and θ, ϱ obeys the Gamma distribution with parameters equal to Nk and θ. Next, define

$\mathrm{G} = \left(\sum_{n=1}^{N} |h_{1,n}||g_{1,n}|\right)^2$, one have $\mathrm{G} = \varrho^2$. Hence, by some mathematical manipulations, one can obtain the PDF of G as follows

$$f_{\mathrm{G}}(x) = \frac{1}{2\Gamma(Nk)\theta^{Nk}} x^{\frac{Nk}{2}-1} \exp\left(-\frac{\sqrt{x}}{\theta}\right), \tag{7}$$

In the section II, we assume that $h_{1,n}$ and $h_{2,n}$, $g_{1,n}$ and $g_{2,n}$ have the same fading coefficients α and β, respectively. Therefore, let $\mathrm{Z} = \left(\sum_{n=1}^{N} |g_{2,n}||h_{2,n}|\right)^2$, the PDF of Z can be written as

$$f_{\mathrm{Z}}(z) = \frac{1}{2\Gamma(Nk)\theta^{Nk}} z^{\frac{Nk}{2}-1} \exp\left(-\frac{\sqrt{z}}{\theta}\right), \tag{8}$$

Based on the above results, we continue to derive the PDF and the cumulative distribution function (CDF) of γ in (4).

Lemma 1. The PDF of the instantaneous SNR γ can be given as

$$f_{\gamma}(x) = \frac{x^{\frac{Nk}{2}-1}}{\Gamma^2(Nk)\delta^{\frac{Nk}{2}}\theta^{2Nk}} K_0\left(\frac{2}{\theta}\left(\frac{x}{\delta}\right)^{\frac{1}{4}}\right), \tag{9}$$

where $K_0(\cdot)$ denotes the 0-th order modified Bessel function of the second kind.

Proof: We first define $\zeta = \mathrm{G} \cdot \mathrm{Z}$. Since G and Z are statistically independent of each other, then one can have $f_{\zeta}(\vartheta)$ as

$$\begin{aligned} f_{\zeta}(\vartheta) &= \int_0^{\infty} \frac{1}{x} f_{\mathrm{G}}\left(\frac{\vartheta}{x}\right) f_{\mathrm{Z}}(x)\,\mathrm{d}x \\ &\overset{(a)}{=} \frac{\vartheta^{\frac{Nk}{2}-1}}{4\Gamma^2(Nk)\theta^{2Nk}} \int_0^{\infty} x^{-1} \exp\left(-\frac{\sqrt{\vartheta}}{\theta\sqrt{x}} - \frac{\sqrt{x}}{\theta}\right)\mathrm{d}x \\ &\overset{(b)}{=} \frac{\vartheta^{\frac{Nk}{2}-1}}{\Gamma^2(Nk)\theta^{2Nk}} K_0\left(\frac{2\vartheta^{\frac{1}{4}}}{\theta}\right), \end{aligned} \tag{10}$$

where (a) is obtained by using (6) and (8), (b) follows from [16, Eq. (3.471.9)].

Finally, we can get the result of (9) by using some variable transformation on (4) and (10). ■

Lemma 2. One can have the CDF of γ as follows

$$F_{\gamma}(x) = A \cdot x^{\frac{Nk}{2}} \left(\frac{2 \cdot K_0(B)\,{}_1F_2\left(1; Nk, Nk+1; \frac{B^2}{4}\right)}{Nk} + \frac{B \cdot K_1(B)\,{}_1F_2\left(1; Nk+1, Nk+1; \frac{B^2}{4}\right)}{(Nk)^2}\right), \tag{11}$$

where $A = \frac{1}{\Gamma^2(Nk)\delta^{\frac{Nk}{2}}\theta^{2Nk}}$, $B = \frac{2}{\theta}\left(\frac{x}{\delta}\right)^{\frac{1}{4}}$, $K_1(\cdot)$ is the 1-th order modified Bessel function of the second kind, ${}_pF_q$ denote the generalized hypergeometric function [16].

Proof: By using (9), one can have

$$F_{\gamma}(x) = \frac{1}{\Gamma^2(Nk)\delta^{\frac{Nk}{2}}\theta^{2Nk}} \int_0^{x} y^{\frac{Nk}{2}-1} K_0\left(\frac{2}{\theta}\left(\frac{y}{\delta}\right)^{\frac{1}{4}}\right)\mathrm{d}y, \tag{12}$$

It can be seen from (12) that it is difficult to obtain its closed-form expression directly due to the existence of non-elementary functions. Therefore, similar to [4], in order to conduct the derivation, we first give the derivation of $\int y^{\frac{Nk}{2}-1} K_0\left(\frac{2}{\theta}\left(\frac{y}{\delta}\right)^{\frac{1}{4}}\right)\mathrm{d}y$ as follows

$$\begin{aligned} &\int y^{\frac{Nk}{2}-1} K_0\left(\frac{2}{\theta}\left(\frac{y}{\delta}\right)^{\frac{1}{4}}\right)\mathrm{d}y \\ &\overset{(c)}{=} \frac{\delta^{\frac{Nk}{2}}\theta^{2Nk}}{2^{2Nk-2}} \int \omega^{\frac{Nk}{2}-1} K_0(\omega)\,\mathrm{d}\omega \\ &\overset{(d)}{=} \frac{\delta^{\frac{Nk}{2}}\theta^{2Nk}}{2^{2Nk-2}} \omega^{2Nk} \cdot \left(\frac{K_0(\omega)\,{}_1F_2\left(1; Nk, Nk+1; \frac{\omega^2}{4}\right)}{2Nk} + \frac{\omega K_1(\omega)\,{}_1F_2\left(1; Nk+1, Nk+1; \frac{\omega^2}{4}\right)}{4(Nk)^2}\right) \end{aligned} \tag{13}$$

where (c) is obtained by substituting $\omega = \frac{2}{\theta}\left(\frac{y}{\delta}\right)^{\frac{1}{4}}$, (d) follows from [17, Sec. 1.1.2] as well as the definition of ${}_pF_q$. Then, we can obtain (11) by replacing the variable ω to y and substituting the transformed result into (12). In particular, one get (11) given that $\lim_{y\to 0} y^{\frac{Nk}{2}-1} K_{\tau}\left(\frac{2}{\theta}\left(\frac{y}{\delta}\right)^{\frac{1}{4}}\right) = 0$, $Nk > 3$, $\tau \in \{0,1\}$, which comes from its series expansion at $y = 0$ [4]. Hence, **Lemma 2** holds. ■

By inserting (9) into (5), one sees that it is intractable to obtain a closed-form solution of (5) due to the existence of the $Q(\cdot)$. Therefore, we approximate the Q function in formula (5) as a linear function. Then, one have [14]

$$\begin{aligned} &Q\left(\ln 2\sqrt{\frac{v}{V(\gamma)}}\left(\log_2(1+\gamma) - R_s\right)\right) \\ &\approx \begin{cases} 1 & x < x_0 - \frac{1}{2\mu_s} \\ \frac{1}{2} - \mu_s(x - x_0) & x_0 - \frac{1}{2\mu_s} \le x \le x_0 + \frac{1}{2\mu_s} \\ 0 & x > x_0 + \frac{1}{2\mu_s} \end{cases}, \end{aligned} \tag{14}$$

where $\mu_s = \sqrt{\frac{v}{2\pi(2^{2R_s}-1)}}$ and $x_0 = 2R_s - 1$.

Lemma 3. The APEP $\bar{\varepsilon}$ is derived in a closed-form as

$$\begin{aligned} \bar{\varepsilon} \approx\ & F_{\gamma}\left(x_0 - \frac{1}{2\mu_s}\right) + \left(\frac{1}{2} + \mu_s x_0\right) \cdot \\ & \left(F_{\gamma}\left(x_0 + \frac{1}{2\mu_s}\right) - F_{\gamma}\left(x_0 - \frac{1}{2\mu_s}\right)\right) \\ & - \mu_s \cdot \left(U\left(x_0 + \frac{1}{2\mu_s}\right) - U\left(x_0 - \frac{1}{2\mu_s}\right)\right), \end{aligned} \tag{15}$$

where $F_{\gamma}(\cdot)$ is given in **Lemma 2**, $U(\cdot)$ is given as follows

$$U(x) = A \cdot x^{\frac{Nk}{2}+1} \left(\frac{2 \cdot K_0(B)\,{}_1F_2\left(1; Nk+2, Nk+3; \frac{B^2}{4}\right)}{Nk+2} + \frac{B \cdot K_1(B)\,{}_1F_2\left(1; Nk+3, Nk+3; \frac{B^2}{4}\right)}{(Nk+2)^2}\right), \tag{16}$$

and A, B, $K_0(\cdot)$, $K_1(\cdot)$ as well as ${}_1F_2$ are defined in **Lemma 1** and **Lemma 2**.

Proof: By plugging (14) and (9) into (5), one can have

$$\bar{\varepsilon} \approx \frac{1}{\Gamma^2(Nk)\,\delta^{\frac{Nk}{2}}\theta^{2Nk}} \cdot \Bigg(\underbrace{\int_0^{x_0-\frac{1}{2\mu_s}} x^{\frac{Nk}{2}-1} K_0\left(\frac{2}{\theta}\left(\frac{x}{\delta}\right)^{\frac{1}{4}}\right) dx}_{S_1} + \left(\frac{1}{2}+\mu_s x_0\right) \cdot \underbrace{\int_{x_0-\frac{1}{2\mu_s}}^{x_0+\frac{1}{2\mu_s}} x^{\frac{Nk}{2}-1} K_0\left(\frac{2}{\theta}\left(\frac{x}{\delta}\right)^{\frac{1}{4}}\right) dx}_{S_2} - \mu_s \underbrace{\int_{x_0-\frac{1}{2\mu_s}}^{x_0+\frac{1}{2\mu_s}} x^{\frac{Nk}{2}} K_0\left(\frac{2}{\theta}\left(\frac{x}{\delta}\right)^{\frac{1}{4}}\right) dx}_{S_3} \Bigg), \tag{17}$$

where S_1 and S_2 can be obtained with the help of (13), S_3 can be converted to (16) by some algebraic operations on (13).

Therefore, one can get (15) by inserting the obtained results of S_1, S_2 and S_3 into (17). ■

Algorithm 1 GA for obtaining solution of the problem (19)

Input: population size $M = 200$, selected rate $r_s = 0.9$, crossover rate $r_c = 0.4$, mutation rate $r_m = 0.2$, iterations $M_{iters} = 40$

Output: the optimal values of m, v and $\bar{\varepsilon}$

1: $gen := 1$
2: **while** $gen < M_{iters}$ **do**
3: Calculate fitness by using (15) and (19).
4: Choose the $M * r_s$ individuals in ascending fitness order as the best individuals.
5: *Select* the individuals by using the roulette wheel.
6: Perform the *crossover* operation by using one point crossover.
7: Perform the *mutation* operation by applying random changes, mating generates new offspring.
8: The above 3 basic operation individuals plus the best individuals carry out the next iteration together.
9: **end while**

IV. Effective Throughput

By using (15), the ET of the system can be expressed as

$$\psi = R_s\left(1-\bar{\varepsilon}\right) \tag{18}$$

Our goal is to jointly optimize the channel uses in the WET and WIT phase to maximize the ET of the system. For a given transmission power of the HAP, we establish the following ET maximization problem under the latency constraint

$$\max_{m,v} \quad \psi \tag{19}$$

$$s.t.\,(m+v)\,T_c \le T_s \tag{19a}$$

$$m, v \in \mathbb{N}^+ \tag{19b}$$

where $\mathbb{N}^+$ represents the positive integer set and T_s is the latency of a "harvest and then transmit" process. $(19a)$ is the latency constraint and $(19b)$ indicates that the number of channel uses should be a positive integer.

Note that (19) is an integer programming problem and it is difficult to address it. One can use the exhaustive search to get the optimal solution, but it is inefficient to do so. To this end, we apply a GA [18] based algorithm to deal with it. We describe the GA in Algorithm 1.

V. Numerical Results and Discussions

In this section, we verify the accuracy of our results in (15) through Monte-Carlo simulations. Unless otherwise specified, the simulation parameters are set as follows: $\eta = 0.3$, $L = 500$ bits, $\sigma_{\mathrm{I}}^2 = -94$ dBm, $T_c = 3$ μs and $T_s = 0.9$ ms. Moreover, we consider a 3-dimensional (3D) Cartesian coordinate in meters, where the HAP is located at $(0,0,0)$, the device is at $(30,0,0)$ and the IRS is located at $(30,4,3)$. Similar to [11], we model the fading coefficient [dB] as follows: $\alpha = G_t + G_r + 37.6\log_{10}(d_{\mathrm{HI}}) - 30$ and $\beta = G_t + G_r + 37.6\log_{10}(d_{\mathrm{ID}}) - 30$, where $G_t = 3.2$ dBi and $G_r = 1.3$ dBi are the antenna gain at the transmitter and receiver, respectively; d_{HI} is the distance between the HAP and IRS, and d_{ID} is the distance between the IRS and device. The curves labelled 'Simulation' are obtained by averaging over 10^9 random samples. The curves corresponding to 'Numerical' and 'Approximation' are given in (5) and (15), respectively.

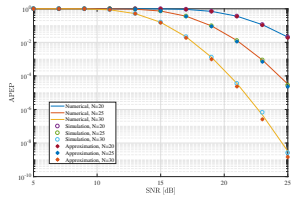

Fig. 2. Performance analysis of APEP versus SNR.

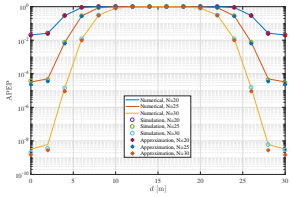

Fig. 3. APEP performance in terms of changing the IRS location at (d,4,3).

Fig. 2 depicts the APEP versus SNR under different N. We set $m = 50$ and $v = 50$. Note that in the case of $N = 30$, with the increase of SNR, there is a small gap between the 'Approximation' and 'Numerical' curves. This is due to the linear approximation of (14). It is observed from Fig. 2 that the APEP decrease with the increase of SNR, as expected. In addition, for the same SNR, lager values of N also yield better APEP performance.

In Fig. 3, the APEP results are illustrated for $d \in [0,30]$, where the IRS is located at $(d,4,3)$ on the 3D space. We set SNR $= 10$ dB, $m = 50$ and $v = 50$ in this figure. It can be seen that the APEP behavior is symmetrical with respect to the distance of the HAP or device. In addition, the APEP increases as the IRS moves away from the HAP or device, and the performance is worst when the distances from the IRS to the HAP and the device are equal. This is because the path loss is directly proportional to the product of the distances from the IRS to the HAP and device.

In Fig. 4, we analyze the impact of parameters m and v on system performance with the SNR as 10 dB. In particular, we fix $v = 50$ in Fig. 4(a) and Fig. 4(c), while $m = 50$ in Fig. 4(b) and Fig. 4(d). As shown in Fig. 4(a) and Fig. 4(b), APEP decreases with the increase of m or v, and a lager

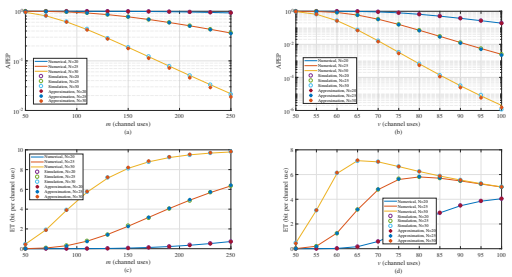

Fig. 4. Performance analysis of parameters m and v with SNR as 10 dB.

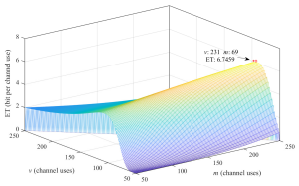

Fig. 5. Performance analysis of ET versus blocklength.

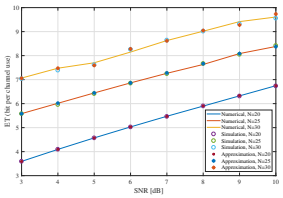

Fig. 6. Performance analysis of ET versus SNR.

N increases the interval between difference curves. As shown in Fig. 4(c), lager values of m or N significantly improve the performance of ET. Note that with the increase of m, ET eventually approaches R_s, which can be seen from the curve of $N = 30$ in the Fig. 4(c). In Fig. 4(d), it observed that there exists a trade off between the parameter v and data rate R_s, since with too small v result in higher APEP, while too large v leads to small data rate. Especially, the curves in the Fig. 4(d) eventually coincide when the value of v is large. This is because the APEP is at a very small level when v is large, and the data rate R_s dominates ET.

In Fig. 5, we plot the ET versus m and v with $N = 20$ and SNR $= 10$ dB. The point indicated by "o" is obtained by the GA in Algorithm 1. As a contrast, the point represented by "$*$" is obtained by applying exhaustive search algorithm, which can be regarded as the optimal solution. However, the exhaustive search algorithm tries to search all feasible solutions, which has the lowest efficiency. It can be seen from Fig. 5 that the optimal values of ET obtained by the two algorithms are consistent, i.e., $m = 231$ and $v = 69$.

In Fig. 6, we illustrate performance of ET versus SNR for different N. Each value of ET in the graph is obtained by solving problem (19) with the GA proposed in Algorithm 1. The curves corresponding to 'Numerical' and 'Approximation' are obtained by taking (5) and (15) as fitness function of the GA respectively. One can see that higher SNR yields better ET. Also, one can see that for a given latency constrain and transmission power at the HAP, the performance of ET can be improved with the increase of the element of IRS.

VI. Conclusion

This paper has investigated the APEP and ET of the IRS-aided uRLLC system supported by WET technology under FBC regime to meet the latency and reliability requirements. An approximate closed-form expression of the APEP is obtained and the best values of channel uses in the WET and WIT phases with the objective of maximizing the ET have been obtained by applying the GA. The effectiveness of the solution has been verified by the simulation. As a future work, we can extend the IRS-assisted uRLLC supported by WET technology to multi-user system, where all the users are located at arbitrary locations in the system. In addition, all the devices and the HAP can be equipped with multiple antennas.

References

[1] L. Zhang, M. Xiao, G. Wu, M. Alam, Y.-C. Liang, and S. Li, "A Survey of Advanced Techniques for Spectrum Sharing in 5G Networks," *IEEE Wireless Commun.*, vol. 24, no. 5, pp. 44–51, Oct. 2017.

[2] J. Hu, K. Yang, G. Wen and L. Hanzo, "Integrated Data and Energy Communication Network: A Comprehensive Survey," *IEEE Commun. Surveys Tuts.*, vol. 20, no. 4, pp. 3169-3219, 4th Quart., 2018.

[3] T. A. Khan, R. W. Heath and P. Popovski, "Wirelessly Powered Communication Networks With Short Packets," *IEEE Trans. Commun.*, vol. 65, no. 12, pp. 5529-5543, Dec. 2017.

[4] O. L. A. López, H. Alves, R. D. Souza and E. M. G. Fernández, "Ultra-reliable Short-Packet Communications With Wireless Energy Transfer," *IEEE Signal Process. Lett.*, vol. 24, no. 4, pp. 387-391, April 2017.

[5] C. Pan, et al, "Reconfigurable Intelligent Surfaces for 6G Systems: Principles, Applications, and Research Directions," *IEEE Commun. Mag.*, 2021. [Online]. Available: https://arxiv.org/abs/2011.04300.

[6] M. Nemati, J. Park and J. Choi, "RIS-Assisted Coverage Enhancement in Millimeter-Wave Cellular Networks," *IEEE Access*, vol. 8, pp. 188171-188185, Oct. 2020.

[7] C. Pan, et al, "Multicell MIMO Communications Relying on Intelligent Reflecting Surfaces," *IEEE Trans. Wireless Commun.*, vol. 19, no. 8, pp. 5218-5233, Aug. 2020.

[8] M. Nemati, B. Maham, S. R. Pokhrel and J. Choi, "Modeling RIS Empowered Outdoor-to-Indoor Communication in mmWave Cellular Networks," *IEEE Trans. Commun.*, doi: 10.1109/TCOMM.2021.3104878.

[9] Ramin Hashemi, Samad Ali, Nurul Huda Mahmood and Matti Latva-aho, "Average Rate and Error Probability Analysis in Short Packet Communications over RIS-aided URLLC Systems," Feb. 2021. [Online]. Available: https://arxiv.org/abs/2102.13363.

[10] S. Gong, C. Xing, S. Wang, L. Zhao and J. An, "Throughput Maximization for Intelligent Reflecting Surface Aided MIMO WPCNs With Different DL/UL Reflection Patterns," *IEEE Trans. Signal Process.*, vol. 69, pp. 2706-2724, April 2021.

[11] T. Van Chien, L. T. Tu, S. Chatzinotas and B. Ottersten, "Coverage Probability and Ergodic Capacity of Intelligent Reflecting Surface-Enhanced Communication Systems," *IEEE Commun. Lett.*, vol. 25, no. 1, pp. 69-73, Jan. 2021.

[12] Q. Wu and R. Zhang, "Towards Smart and Reconfigurable Environment: Intelligent Reflecting Surface Aided Wireless Network," *IEEE Commun. Mag.*, vol. 58, no. 1, pp. 106-112, Nov. 2020.

[13] C. You, B. Zheng and R. Zhang, "Channel Estimation and Passive Beamforming for Intelligent Reflecting Surface: Discrete Phase Shift and Progressive Refinement," *IEEE J. Sel. Areas Commun.*, vol. 38, no. 11, pp. 2604-2620, Nov. 2020.

[14] K. Wang, C. Pan, H. Ren, W. Xu, L. Zhang and A. Nallanathan, "Packet Error Probability and Effective Throughput for Ultra-Reliable and Low-Latency UAV Communications," *IEEE Trans. Commun.*, vol. 69, no. 1, pp. 73-84, Jan. 2021.

[15] H. Ren, K. Wang and C. Pan, "Intelligent Reflecting Surface-aided URLLC in a Factory Automation Scenario," Mar 2021. [Online]. Available: https://arxiv.org/abs/2103.09323.

[16] I. S. Gradshteyn and I. M. Ryzhik, *Table of Integrals, Series and Products*, 7th. San Diego, CA: Academic Press, 2007.

[17] W. Rosenheinrich, "Tables of some indefinite integrals of bessel functions," University of Applied Sciences, Jena, Germany, 2012. [Online]. Available: https://ftp.emc.ncep.noaa.gov/mmb/wd20ww/cp-tmp/besint.pdf.

[18] S. Li, J. Yang, W. Song and A. Chen, "A Real-Time Electricity Scheduling for Residential Home Energy Management," *IEEE Internet Things J.*, vol. 6, no. 2, pp. 2602-2611, April 2019.